Atmos. Meas. Tech. Discuss., 4, 6643–6678, 2011
www.atmos-meas-tech-discuss.net/4/6643/2011/
doi:10.5194/amtd-4-6643-2011

Atmospheric Measurement Techniques Discussions

Long-term aerosol optical depth datasets over China retrieved from satellite data

Y. Xue[1,2], H. Xu[1,3], Y. Li[1,3], L. Yang[4,5], L. Mei[1,3], J. Guang[1], T. Hou[3,6], X. He[1,3], J. Dong[1,3], Z. Chen[3,6], and Y. Qi[7]

[1]State Key Laboratory of Remote Sensing Science, Jointly Sponsored by the Inst. of Remote Sensing Applications of Chinese Academy of Sciences and Beijing Normal University, Inst. of Remote Sensing Applications, Chinese Academy of Sciences, Beijing, China
[2]Faculty of Computing, London Metropolitan University, 166-220 Holloway Road, London N7 8DB, UK
[3]Graduate University of Chinese Academy of Sciences, Beijing 100049, China
[4]School of Geography, Beijing Normal University, Beijing 100875, China
[5]School of Surveying and Land Information Engineering, Henan Polytechnic University, Jiaozuo 454003, China
[6]Center for Earth Observation and Digital Earth of the Chinese Academy of Sciences, Beijing 100094, China
[7]School of Economics and Management, Beijing Forestry University, Tianjin, China

Received: 30 September 2011 – Accepted: 23 October 2011 – Published: 3 November 2011

Correspondence to: Y. Xue (yxue@irsa.ac.cn)

Abstract

Nine years of daily aerosol optical depth (AOD) measurements have been derived from the Moderate Resolution Imaging Spectroradiometer (MODIS) data using the Synergetic Retrieval of Aerosol Properties (SRAP) method over China for the period from August 2002 to August 2011, comprising AODs at 470, 550, and 660 nm. Then, the variation over China over the nine years was determined from the derived AOD data. Preliminary daily results show the agreement between the Aerosol Robotic Network (AERONET) AOD data and the derived AOD data. From 1219 daily collocations, representing mutually cloud-free conditions, we find that more than 54 % of SRAP-MODIS retrieved AOD values comparing with AERONET-observed values within an expected error envelop of 20 %. From 222 monthly averaged collocations, representing mutually cloud-free conditions, we find that more than 63 % of SRAP-MODIS retrieved AOD values comparing with AERONET-observed values within an expected error envelop of 15 % and more than 70 % within an expected error envelop of 20 %. In addition, the long-term SRAP AOD dataset has been implemented in analysing case studies involving dust storms, haze and the characteristics of AOD variation over China over the past nine years. It was found that areas in China with high AOD values generally appear in the Inner Mongolia, the North China Plain, Tarim Basin, the Sichuan Basin, the Tibetan Plateau and the middle and lower reaches of the Yangtze River and area with low AOD values generally appear in the Fujian Province, the Yungui Plateau, and northeast plain. The seasonal averaged AOD results indicate that AOD values generally reach their maximum in spring and their minimum in winter. The yearly mean and monthly mean SRAP AOD were also used to study the spatial and temporal aerosol distributions over China. The results indicate that the AOD over China exhibited no obvious change. Monthly averaged AOD in August in Beijing experienced one decreasing processes from 2006 to 2010, especially after 2007. The monthly mean AOD decreased from 0.46 in 2007 to 0.29 in 2010.

AMTD

4, 6643–6678, 2011

SRAP AODs were used to study one haze case and dust case. Combining AOD data from the SRAP AOD dataset and HYSPLIT model can forecast the transport of haze. SRAP AOD data are also sensitive enough to reflect the occurrence and intensity of dust weather. Thus, the SRAP AOD dataset can be used to precisely reflect the spatial distribution, concentration distribution and transmission path of dust.

1 Introduction

Aerosols affect our environment at the local, regional, and global level. It is very important to build a complete picture of aerosols across the globe so that we may understand how they vary both in time and space. It is even more important, however, that such observations be on-going so we may monitor any build-ups that may be occurring. After all, because our present climate is a reflection of our current atmosphere – including its greenhouse gases and aerosols – it is the changes in these components that will lead to climate change. Before the satellite era, information regarding aerosols came from limited surface-based observations, which are not sufficient to describe the spatial and temporal variability of aerosols (Levy and Pinker, 2007). The only way to achieve on-going global coverage is by satellite observation.

Aerosols could be sampled remotely by satellite, but only indirectly, by means of a combination of various wavelengths of upwelling radiation (Rosenfeld and Lensky, 1998). Even then, numerous assumptions are required. The determination of the aerosol optical depth from satellite remote-sensing measurements is extremely complex due to the large variability of aerosol optical properties. Significant simplification occurs when measurements are taken over water because the ocean reflection signal can be neglected in the near-infrared spectrum. Unfortunately, over land, most of the signal can be attributed to ground reflectance.

For years, many algorithms have been applied to these satellite datasets to retrieving information useful for studying aerosol over land (Kokhanovsky et al., 2007; Kokhanovsky and de Leeuw, 2009). In this paper, we used a new approach called the

AMTD
4, 6643–6678, 2011

Synergetic Retrieval of Aerosol Properties (SRAP) method to determine aerosol properties over land surfaces, especially high-reflectance surfaces including arid, semiarid, and urban areas (Xue and Cracknell, 1995). The algorithm developed makes full use of the high frequency multi-temporal information and multi-spectral information from the Moderate Resolution Imaging Spectroradiometer (MODIS) without any prior knowledge of the underlying land surface characteristics (Tang et al., 2005). The quantitative retrieval of the aerosol optical depth (AOD) from satellite data for land surface has been successfully conducted for China using MODIS data. Fused with the national aerosol measurement network data, the long-term national AOD maps at 10 and 1 km resolutions have been produced on the daily base. This national climate AOD data will be useful for the research of regional response to the global climate change. The SRAP method, data and processing is introduced in Sects. 2 and 3, respectively; validation strategy is performed in Sect. 4; results of case study and the long-term trend are provided in Sect. 5 and summary and conclusions are given in the closing section.

We considered four seasons: spring (MAM), summer (JJA), autumn (SON), and winter (DJF). Parameters used in this study include AOD at 550 nm and Angstrom exponent. All products are given at a spatial resolution of $0.1^{\circ} \times 0.1^{\circ}$.

2 Method

The SRAP model is a simple algorithm because the AOD is calculated from the atmospheric radiative transfer equation without a look-up table (LUT), and almost all input data can be obtained from remote-sensing data. However, it is a practical algorithm. We used this algorithm to retrieve AODs from MODIS data from August 2002 to August 2011.

Xue and Cracknell (1995) determined the relation between the ground surface reflectance A and the apparent reflectance (reflectance on the top of atmosphere) A' to be as follows:

AMTD
4, 6643–6678, 2011

$$A = \frac{(2A' - \sec\theta) + \sec\theta(1 - A')e^{(\sec\theta - 2)\varepsilon\tau_0^\lambda \sec\theta'}}{(2A' - \sec\theta) + 2(1 - A')e^{(\sec\theta - 2)\varepsilon\tau_0^\lambda \sec\theta'}} \quad (1)$$

where ε is the backscattering coefficient, typically 0.1; τ_0 is the optical depth of the whole atmosphere.

For our model SRAP, which only takes into account the scattering of atmospheric molecular and aerosol particles, we assume that the atmospheric optical thickness τ_0^λ consists of two parts: the molecular Rayleigh scattering $\tau_M^\lambda(\infty)$ and the scattering of aerosol particles $\tau_A^\lambda(\infty)$. Therefore, the dimensionless quantity of the optical thickness of the whole atmosphere is as follows:

$$\tau_0^\lambda = \tau_M^\lambda(\infty) + \tau_A^\lambda(\infty) \quad (2)$$

The molecular Rayleigh scattering and the aerosol particle scattering can be expressed as follows:

$$\tau_M^\lambda = 0.00879\lambda^{-4.09} \quad (3)$$

$$\tau_A^\lambda = \beta\lambda^{-\alpha} \quad (4)$$

Following Eqs. (1)–(4), we assumed that, for two MODIS observations within short time intervals between the overpasses of Terra and Aqua, the ground surface bidirectional reflectance properties and aerosol types and properties (α) did not change. Flowerdew and Haigh (1995) proposed that the surface reflectance be approximated by the variation in the wavelength and the variation in the geometry. Under this assumption, the ratio of the surface reflectance from both Terra MODIS and Aqua MODIS in morning and early afternoon can be expressed as follows:

$$K_{\lambda_i} = \frac{A_{1,\lambda_i}}{A_{2,\lambda_i}} \quad (5)$$

where $i = 1, 2$ indicates the observation of Terra MODIS and Aqua MODIS, respectively. Three visible bands (0.47, 0.55, and 0.66 m) of MODIS were used to retrieve the AOD

AMTD
4, 6643–6678, 2011

data. The method has been described in detail by Tang et al. (2005). This has proved to be an effective method (Mei et al., 2011), even for high-latitude areas.

3 Data and processing

This section describes the remote-sensing data, field measurements used for validation and auxiliary data used for analysis, and the data processing.

3.1 Satellite data

MODIS is a next generation imaging spectroradiometer that has a moderate spectral resolution, with 36 spectral bands covering wavelengths from 0.4 to 14 µm, three spatial resolutions of 250, 500 and 1000 m and a swath of 2330 km. MODIS AOD data were retrieved using multiple channels from the MODIS sensors aboard the Terra and Aqua satellites beginning in 2000 and 2002, respectively. MODIS Level 1 and atmosphere data are available through the LAADS website (http://modis.gsfc.nasa.gov/data/).

We used Terra and Aqua MODIS data obtained between August 2002 and August 2011 over China, including L1B Calibrated data MOD/MYD02, geo-location data MOD/MYD03 and cloud mask product MOD/MYD35. All MODIS data have a resolution of 10 km × 10 km.

3.2 The Aerosol Robotic Network (AERONET) data

AERONET provides globally distributed observations of spectral AODs for three data quality levels: Level 1.0 (unscreened), Level 1.5 (cloud-screened), and Level 2.0 (cloud-screened and quality-assured). Ten AERONET sites in the region of interest were used from 1 August 2002 to 31 December 2010. The cloud-screened Level 1.5 AOD data available from AERONET in China were collected during these ten years for comparison with the long-term AOD dataset. However, there were no AERONET measurements at the MODIS wavelengths of 0.47, 0.55 and 0.66 µm. The AOD at

0.5 µm was chosen for further analysis. If there was no AOD value at 0.5 µm, those at 0.675 µm were used. Figure 1 shows the AERONET sites in the study area. Table 1 shows the information regarding the latitude, longitude and elevation of selected AERONET sites. Beware that we only use those collocations with mutually cloud-free conditions.

3.3 HYSPLIT data

The HYSPLIT (HYbrid Single-Particle Lagrangian Integrated Trajectory) model is a complete system for computing simple air parcel trajectories and complex dispersion and deposition simulations. HYSPLIT can compute the advection of a single pollutant particle or its trajectory (http://www.arl.noaa.gov/HYSPLIT_info.php). In this research, HYSPLIT was used to characterise the transport of air mass over the study area. Some studies of aerosol transport tend to depict transport as if it has occurred all at one level, making trajectories especially useful.

3.4 Data processing

The steps used to retrieve AODs included cloud mask, geo-reference, and AOD calculations. This process is illustrated in Fig. 2.

Step 1 Cloud mask. We chose the MODIS cloud mask product MOD/MYD35 to mask the MODS L1B data.

Step 2 Geo-reference. Because our algorithm is based on the pixels of both satellite data, the registration is very important.

Step 3 AOD calculation. Because the equations are too difficult to obtain the analytic solutions, we used the Levenberg-Marquardt method to obtain a numerical solution.

For AOD retrieval, which is a data-intensive computational application, we introduced the AOD retrieval Grid workflow to help us to improve the computational efficiency. The

Condor Pool shown in Fig. 3 is at the Institute of Remote Sensing Applications, Chinese Academy of Sciences (Xue et al., 2011). It consists of 40 personal computers (PCs) with 93 central processing units (CPUs), as some PCs are dual-core computers.

4 Validation strategy

The primary source of validation data for the AOD datasets derived from satellite measurements is the AERONET database, which consists of a worldwide network of automated standard sun photometers. Such measurements are the most direct way of determining the column AOD, and the common analysis and quality control of the AERONET database makes it a powerful validation tool. A comparison between the SRAP AOD dataset and AERONET AOD data from 2010 for 550 nm band has been done. The two datasets show a high degree of correlation (R) and a low root-mean-square (RMS) difference From those 1219 collocations (Fig. 4), representing mutually cloud-free conditions, we find that more than 54 % of SRAP-MODIS retrieved AOD values comparing with AERONET-observed values within an expected error envelop of 20 %.

We also validated SRAP-MODIS AOD dataset with AOD measurements at 4 AERONET sites (Beijing, Xianghe, Lulin and Hong_Kong_Hok_Tsui) in China. Figure 5 shows the relationships between monthly averaged SRAP AODs and monthly averaged AERONET AODs for the 550 nm with a resolution of 10 km × 10 km over Asia at four sites. Figure 6 shows the relationships between monthly averaged SRAP AODs and monthly averaged AERONET AODs for the 550 nm with a resolution of 10 km × 10 km over Asia for 2002 to 2011. From those 222 collocations, representing mutually cloud-free conditions, we find that more than 57 % of SRAP-MODIS retrieved AOD values comparing with AERONET-observed values within an expected error envelop of 15 % for Terra satellite and more than 69 % for Aqua satellite. Also, we find that more than 64 % within an expected error envelop of 20 % for Terra satellite and more than 76 % for Aqua satellite. Overall, we find that more than 63 % of derived AOD

AMTD
4, 6643–6678, 2011

values within an expected error envelop of 15 % and more than 70 % within an error envelop of 20 %.

5 Case study and the long-term trend analysis

5.1 Case study

5.1.1 Case study of haze monitor

Smog frequently builds up in Eastern China during the winter, when weather conditions trap pollutants over the plain. Thick haze and fog settled over much of China on 28 October 2009. The thickest of the gray-brown haze conformed to the low-lying contours of the Yellow River Valley and the western half of the North China Plain near the Luliang Mountains (http://earthobservatory.nasa.gov/NaturalHazards). In Fig. 7a, an Aqua MODIS RGB composite image (enhanced by Gaussian method) of the study area on 28 October 2009 is shown. Figure 7b shows the AODs at 550 nm from the SRAP AOD dataset. We can see that the areas covered by heavy fog have high AOD values, usually higher than 0.8. The high AODs were distributed over Hebei, Shandong and other Yellow River plain areas, where the altitudes are very low. The fog may be much heavier due to temperature inversion (Garreaud et al., 2008). Usually, cold air is located in high-altitude areas, but sometimes, it may be driven under warm air. Because of the high density of cold air and calm wind, it is difficult for the two layers of air to mix together. As a result, the pollutants in the cold air near the surface can persist for a long time.

Combining the AOD data from the SRAP AOD dataset and HYSPLIT model can be used to forecast the transport of haze. The AOD results can index the fog scope, geographic distribution and the relative thickness. To study this variability of the heavy fog on 28 October 2009 in greater detail, we used AODs at 550 nm from the SRAP AOD dataset on 26 October 2009 (Fig. 8a). We also used HYSPLIT forward trajectories

AMTD
4, 6643–6678, 2011

to determine the transport path of air masses on 26 October 2009 with two different origins: Hebei Province (38.6° N, 115.5° E) and Hubei Province (31.1° N, 115.1° E) (Fig. 8b). From Fig. 8a,b, we can infer that the high AODs should move northeast in the Hebei province and move northern in the Anhui province, which is consistent with the trajectories' transport line. Combining the AOD data from the SRAP AOD dataset and HYSPLIT model can be used to forecast the transport of haze.

5.1.2 Case study of dust monitoring

Sand storms often occur in deserts and their surrounding borders. The northwest arid region of China is one of the most frequently affected regions. Dust aerosol, which vastly exists in the dust in this area, affects the balance of radiation and energy through the absorption and scattering of solar radiation and ground and cloud long-wave radiation, which also affects the atmospheric turbidity value.

A strong dust transport process occurred in China during 19–23 March 2010, which extended the area affected from Northern China to the Yangtze River and its southern region. According to the ground-based monitor, the main source region was located southwest of Mongolia, at the Sino-Mongolian border and in the Southern Xinjiang Basin. The dust weather, which is associated with Mongolian cyclones and the transit of strong cold air, was strengthened during its transport to Gansu Province and Inner Mongolia, affecting the middle and lower reaches of the Yangtze River, the south Yangtze River regions and southeast coastal area.

Figure 9 shows the distribution of dust-type AODs between 21 and 22 March 2010. The dust-type AODs were obtained using the combing AOD retrieved by SRAP at 550 nm and the aerosol classification method proposed by Barnaba and Gobbi (2004). Figure 9a shows that the China-Mongolia border region, one of the source regions, has high AOD values. Meanwhile, Fig. 9b shows the appearance of dust-type aerosol over another source region – the South Xinjiang Basin.

On 21 March 2010, dust weather moved continually southward, affecting the middle and lower Yangtze, Yangtze River regions and southeast coastal areas. Shanghai,

AMTD
4, 6643–6678, 2011

Nanjing, Suzhou and other cities suffered heavy pollution; Jinan, Zaozhuang and other cities suffered moderate heavy pollution; and Changsha, Xiangtan and other cities suffered slight pollution. The linear high AOD value zone shown in Fig. 9a visually indicates that the transmission path of dust aerosol moves eastward from west to the junctional zone of the East China Sea and the Yellow Sea, as far as Japan. Furthermore, the Air Pulltion Index (API) value overlay map also reflects the transfer path of dust, which is consistent with the satellite AOD result.

On 22 March 2010, from morning until the afternoon, Nanjing, Hangzhou, Taizhou and other cities suffered heavy pollution; Beijing, Ningbo, Shenzhen, and other cities suffered moderate to heavy pollution; and Suzhou and Jiujiang suffered slight pollution. From Fig. 9b, which shows the AOD results, it can be seen that dust was transported along the southeast coastal regions, and the high AOD values were mainly distributed in the East China Sea and South China Sea as well as its coastal region. This result is consistent with the API results, which show high API values over the Southeast Coastal Zone in China. According to the analysis of the HYSPLITE backward trajectory shown in Fig. 10, the transmission path is in agreement with the transmission route revealed by dust-type aerosol.

5.2 Summary of aerosol distributions in China

5.2.1 The characteristics of AOD variation over China over the past nine years

Figure 11 shows the averaged AOD values between 2003 and 2010. High-value areas include the Inner Mongolia, North China Plain, Tarim Basin, Sichuan Basin, Tibetan Plateau, and middle and lower reaches of the Yangtze River, whereas in Fujian Province, the Yungui Plateau and Northeast Plain, the AOD values are low.

The value of AOD is influenced by the production, transport and ultimate fate of aerosol. Human activity is one of the main sources of aerosol. The high AOD values in the North China Plain are caused by this activity. Every year, a large number of crops were burned on farms, leading to heavy pollution. The aerosol values in the

AMTD
4, 6643–6678, 2011

southwest of Xinjiang are distinct in that the northeast part of Xinjiang, which features less vegetation and more deserts, has higher AOD values. Another high-value centre due to desert conditions is located in Inner Mongolia and is connected together with the outside high centre in Mongolia to the north of China. It is estimated that the desert aerosols travelling through this entrance to China make a large contribution to the total aerosol in China. All three desert dust areas mentioned exhibit bright backgrounds resulting from large uncertainties in AOD products, but in the qualitative analysis, the relatively high centres in these deserts are convincing. India, a country to the southwest of China, usually has very high aerosol levels in the summer; however, due to the blocking of paths from India by the Himalayas, the aerosol impact on China may be small. In addition to Inner Mongolia and Guangxi, Xinjiang is another aerosol entrance to China (Li et al., 2003).

The distribution of AOD is not only determined by the source but also depends on the transport of aerosol. Mountains can act as a barrier to the transmission of aerosol and cause the settlement and accumulation of aerosol. Due to the presence of the Dabie Mountains, Huangshan Mountains and some hilly terrains in the middle and lower reaches of the Yangtze River, the AOD distribution pattern shows some high-value centres.

5.2.2 Seasonal aerosol distributions in China

The seasonal distribution of AODs over China averaged from SRAP AOD dataset in the period of 2003–2010 are presented in Fig. 12. In spring, the AOD maxima appeared prominently over the North China Plain and Sichuan Basin. AODs over this area are generally higher than 0.8. Over the middle and lower reaches of the Yangtze River, the AODs are up to 0.6. The AOD values in large region in Inner Mongolia are also high (AOD > 0.4). Zhang et al. (2000) found the maximum AOD values appeared in spring throughout most of China and that the AOD maximum centre exists in the north western part of China due to sandstorms and floating dust. In summer, the AOD values in Northern China are high while the AODs in the Sichuan Basin, the middle and lower reaches of the Yangtze River, and Guangxi are low. The reason is that June is the right season for harvest of wheat in China every year and the period when straw burning takes place seriously in some part of the country. Straw burning happens mainly in winter wheat production area, especially the North China Plain, causing serious pollutions. In autumn, all regions show decreasing trends except Sichuan Basin and the middle and lower reaches of the Yangtze River. In winter, there is a slight increasing trend occurring in the Sichuan Basin and Tibetan Plateau.

Column plot of seasonally averaged AOD at 0.55 nm from SRAP AOD dataset in the period of 2003–2010 is showed in Fig. 13. The AOD maximum appeared in spring over China which is consistent with the conclusion by Liu et al. (2003) who used the MODIS derived AOD products from 2001 to 2002 and found the AOD maximum appeared in spring. The lowest AODs appeared in autumn because aerosol loadings were strongly influenced by northwesterly winds which contributed to the dispersion of tropospheric aerosols.

5.3 Annual variation of AOD over China

Annual mean SRAP AOD data for 2003–2010 is shown in Fig. 14. The annual variation in the AOD over China was mainly analysed with respect to four regions: Beijing (1), Shanghai (2), Chengdu (3) and Guangzhou (4). The distribution of four different regions is shown in Fig. 15.

From Fig. 16, it can be seen that the yearly averaged AODs in Beijing increased from 2004 to 2006 and decreased from 2006 to 2009. The decrease in the aerosol load in Beijing between 2006 and 2009 may be related to China's policies and actions regarding climate change. China has adopted a number of policies and measures to adjust its economic structure, change its development patterns, save energy, raise the efficiency of energy use, optimise energy mixing and promote afforestation. For Chengdu, AODs achieved the highest value in 2006. Different to the trend of AODs over Beijing, AODs over Chengdu increased from 2008 to 2010. The reason for this may be related to the earthquake that occurred in May 2008. For Guangzhou, the

AMTD
4, 6643–6678, 2011

highest AOD average data appeared in 2006, which is consistent with the trend of annual variation in the AODs over whole China. The variation of AODs in Shanghai is not obvious, which reason need further study.

5.4 Monthly trend of AOD data in Beijing

August is chosen to study the monthly trend of AOD in Beijing for the reason that Olympic Games are hosted in Beijing on August, 2008. Beijing is located in the North China Plain which is a grain-producing region with heavily populated, urbanised, and industrialised, containing Hebei, Shandong, and Shanxi provinces. The rapid economic development has increased the consumption of commercial energy in rural areas. As a result, instead of being used for heating energy, more agricultural residues have been directly burned in the field (Cao et al., 2006; He et al., 2007).

Column plot of the AODs in Beijing for August 2002 to August 2010 is shown in Fig. 17. It is worth noting that, monthly averaged AODs in Beijing experienced one decreasing processes from 2006 to 2010, especially after 2007. The monthly mean AODs in August decreased from 0.46 in 2007 to 0.29 in 2010. The decreasing process may be related to the Olympic Games in Beijing. To improve air quality for the 2008 Summer Games, the Chinese government imposed a number of measures in Beijing to reduce the emissions of pollution aerosol. These included temporary closures of factories and restrictions on traffic. Only one half of the approximately 3.3 million registered cars were allowed on the roads each day. The measures were in place from 20 July to 20 September 2008. Within a radius of approximately 150 km around Beijing, similar but less extensive traffic and industry restrictions were imposed (Streets et al., 2008).

AMTD
4, 6643–6678, 2011

6 Discussion and conclusion

The creation of a SRAP AOD dataset is underway, with nine full years of AODs already having been processed. The accuracy of the MODIS-retrieved SRAP AOD dataset over land was evaluated by comparing satellite-based measurements to AERONET ground-based sun photometer observations for different wavelengths (470, 550, and 660 nm) with a resolution of 10 km over Asia. The results of the comparison indicate that the SRAP AOD dataset agrees very well with the AERONET AODs. In most cases, the SRAP AOD data are within approximately 20 % of the AERONET observations.

Currently, the Level 1.0 version of the SRAP AOD datasets is free and available for download at the TGP web site "http://www.tgp.ac.cn". We are working on an extensive and comprehensive validation of the SRAP AOD dataset. We are also working on the quality control and quality assurance of the dataset. The complete Level 1.5 dataset will be produced and become available in mid-2012. In addition, the Level 2.0 AOD dataset integrated with AOD products from other sensors and retrieved with other algorithms will be available soon. This will provide more than ten years of fully validated and quality-controlled AOD data over China.

Acknowledgements. This work was supported in part by the Ministry of Science and Technology (MOST), China under grant nos. 2008AA12Z109, 2010CB950802, and 2010CB950803, and by the Chinese Academy of Sciences under grant no. XDA05100200. The data for validation were obtained from AERONET sites. We thank the PI investigators and their staff for establishing and maintaining these sites used in this investigation.

AMTD

4, 6643–6678, 2011

Long-term aerosol optical depth datasets over China

Y. Xue et al.

References

Barnaba F. and Gobbi, G. P.: Modeling the aerosol extinction versus backscatter relationship for lidar applications: maritime and continental conditions, J. Atmos. Ocean. Tech., 21, 428–442, 2004.

Cao, G. L., Zhang, X. Y., and Zeng, F. C.: Inventory of black carbon and organic carbon emissions from China, Atmos. Environ., 40, 6516–6527, 2006.

Flowerdew, R. and Haigh, J.: An approximation to improve accuracy in the derivation of surface reflectance from multi-look satellite radiometers, Geophys. Res. Lett., 22, 1693–1696, 1995.

Garreaud, R., Barichivich, J., Christie, D. A., and Maldonado, A.: Interannual variability of the coastal fog at Fray Jorge relict forests in semiarid Chile, J. Geophys. Res., 113, G04011, doi:10.1029/2008JG000709, 2008.

He, L. M., Wang, W. J., Wang, Q., Wei, B., Li, Q., Wang, C. Z., and Liu, X. M.: Evaluation of the agriculture residues burning reduction in China using MODIS fire product, Environ. Monit. China, 23, 42–50, 2007.

Kokhanovsky, A. A. and De Leeuw, G. (Eds.): Satellite Aerosol Remote Sensing Over Land, Springer in associated with Praxis Publishing, Chichester, UK, 2009.

Kokhanovsky, A. A., Breon, F.-M., Cacciari, A., Carboni, E., Diner, D., Di Nicolantonio, W., Grainger, R. G., Grey, W. M. F., Höller, R., Lee, K.-H., Li, Z., North, P. R. J., Sayer, A. M., Thomas, G. E., and von Hoyningen-Huene, W.: Aerosol remote sensing over land: a comparison of satellite retrievals using different algorithms and instruments, Atmos. Res., 85, 372–394, 2007.

Levy, R. C. and Pinker R. T.: Remote sensing of spectral aerosol properties: a classroom experience, B. Am. Meteorol. Soc., 88, 25–30, 2007.

Li, C. C., Mao, J. T., Lau Kai-Hon, A., Chen, J. C., Yuan, Z. B., Liu, X. Y., Zhu, A. H., and Liu, G. Q.: Characteristics of distribution and seasonal variation of aerosol optical depth in Eastern China with MODIS products, Chinese Sci. Bull., 48, 2488–2495, 2003.

Luo, Y. F., Lu, D., Zhou, X. J., Li, W. L., and He, Q.: Characteristics of the spatial distribution and yearly variation of aerosol optical depth over China in last 30 years, J. Geophys. Res., 106, 14501–14513, 2001.

Rosenfeld, D. and Lensky, I. M.: Satellite-based insights into precipitation formation processes in continental and maritime convective clouds, B. Am. Meteorol. Soc., 79, 2457–2476, 1998.

Streets, D. G., Fu, J. S., Jang, C. J., Hao, J., He, K., Tang, X., Zhang, Y., Wang. Z., Li, Z., Zhang, Q., Wang, L., Wang, B., and Yu, C.: Air quality during the 2008 Beijing Olympic Games, Atmos. Environ., 41, 480–492, 2007.

Tang, J., Xue, Y., Yu, T., and Guan, Y.: Aerosol optical thickness determination by exploiting the synergy of TERRA and AQUA MODIS, Remote Sens. Environ., 94, 327–334, 2005.

Xue, Y. and Cracknell, A. P.: Operational bi-angle approach to retrieve the Earth surface albedo from AVHRR data in the visible band, Int. J. Remote Sens., 16, 417–429, 1995.

Xue, Y., Chen, Z. Q., Xu, H., Ai, J. W., Jiang, S. Z., Li, Y. J., Wang, Y., Guang, J., Mei, L. L., Jiao, X. J., He, X. W., and Hou, T. T.: A high throughput geocomputing system for remote sensing quantitative retrieval and a case study, Int. J. Appl. Earth Obs., 13, 902–911, 2011.

Zhang, J. H., Wang, M. H., and Mao, J. T.: Error analysis and correction for multi-wavelength sun-photometer aerosol remote sensing, Chinese J. Atmos. Sci., 24, 855–859, 2000.

AMTD
4, 6643–6678, 2011

Long-term aerosol optical depth datasets over China

Y. Xue et al.

Table 1. Selected AERONET stations in the Asian area and their locations (latitude and longitude) for the aerosol retrieval validation.

Number	Name	Latitude (degree north)	Longitude (degree east)	Altitude (m)
1	Bac_Giang	106.225	21.291	15
2	Beijing	39.997	116.381	92
3	Chiang_Mai_Met_Sta	18.771	98.972	312
4	Dalanzadgad	43.577	104.419	1470
5	Dongsha_Island	20.699	116.729	5
6	EPA-NCU	24.968	121.185	144
7	EVK2-CNR	27.959	86.813	5050
8	Gandhi_College	25.871	84.128	60
9	Gosan_SNU	33.292	126.162	72
10	Gual_Pahari	28.426	77.15	384
11	Gwangju_K-JIST	35.228	126.843	52
12	Hong_Kong_Hok_Tsui	22.21	114.258	80
13	Hong_Kong_PolyU	22.303	114.18	30
14	Issyk-Kul	42.623	76.983	1650
15	Kanpur	26.513	80.232	123
16	Karachi	24.87	67.03	49
17	Kathmandu_Univ	27.601	85.538	1510
18	Lahore	31.542	74.325	270
19	Lulin	23.469	120.874	2868
20	Mukdahan	16.607	104.676	166
21	Nainital	29.359	79.458	1939
22	NAM_CO	30.773	90.962	4740
23	NCU_Taiwan	24.967	121.192	171
24	New_Delhi	28.63	77.175	240
25	Osaka	34.651	135.591	50
26	Pune	18.537	73.805	559
27	QOMS_CAS	28.365	86.948	4276
28	Shirahama	33.693	135.357	10
29	Taipei_CWB	25.03	121.5	26
30	Tomsk	56.447	85.047	130
31	XiangHe	39.754	116.962	36
32	Xinglong	40.396	117.578	970

AMTD
4, 6643–6678, 2011

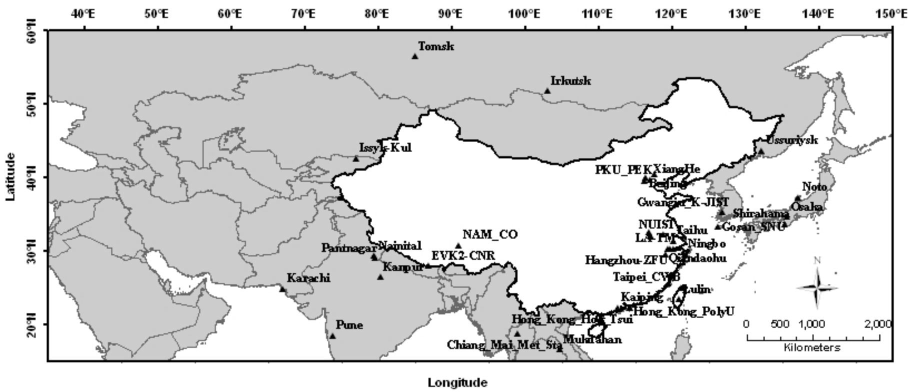

Fig. 1. The AERONET stations in Asia used for the validation of our SRAP AOD datasets.

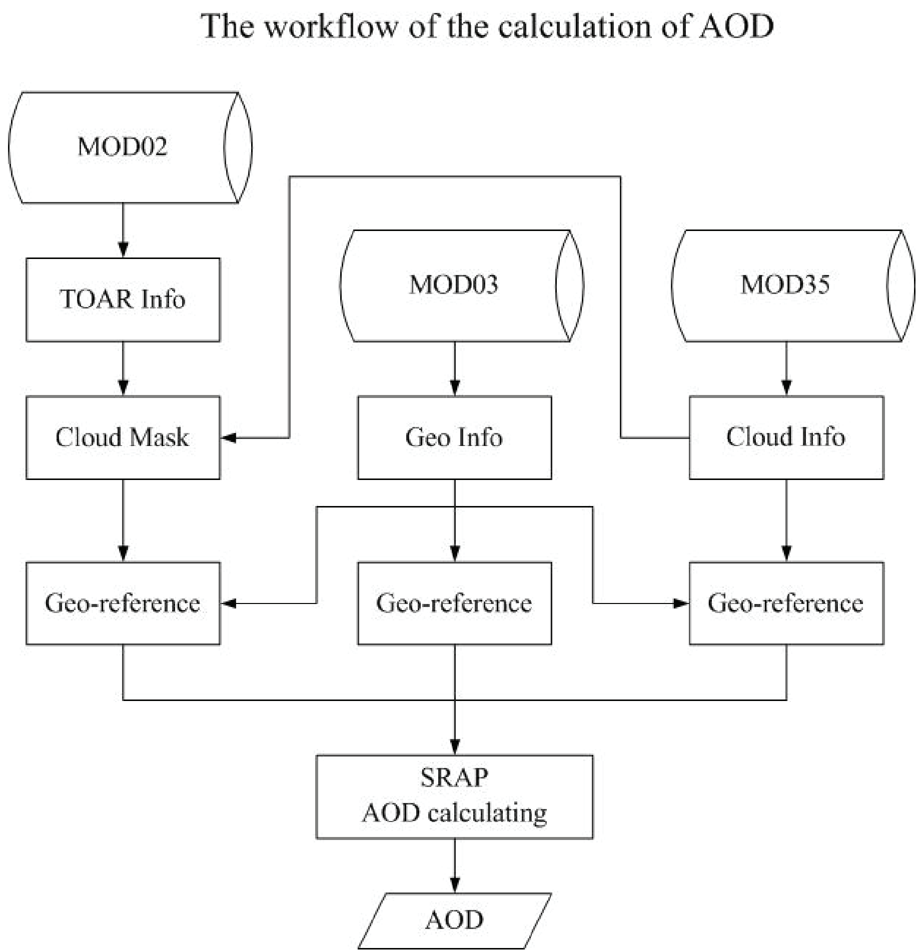

Fig. 2. The workflow of the calculation of AOD.

AMTD
4, 6643–6678, 2011

Fig. 3. Photograph of the Condor Pool.

AMTD
4, 6643–6678, 2011

Long-term aerosol optical depth datasets over China

Y. Xue et al.

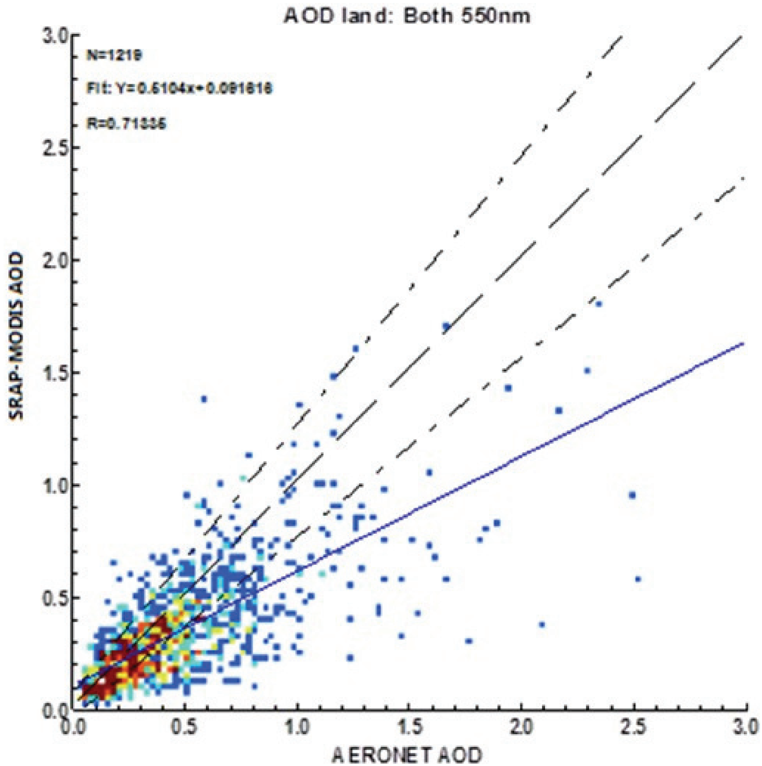

Fig. 4. SRAP-MODIS AOD at 550 nm collocated with AERONET (quadratically interpolated) to the same wavelength, for both (the union of) Terra and Aqua datasets for 2010. Text at the top describes: correlation (R) and the number of collocations, the regression curve.

AMTD
4, 6643–6678, 2011

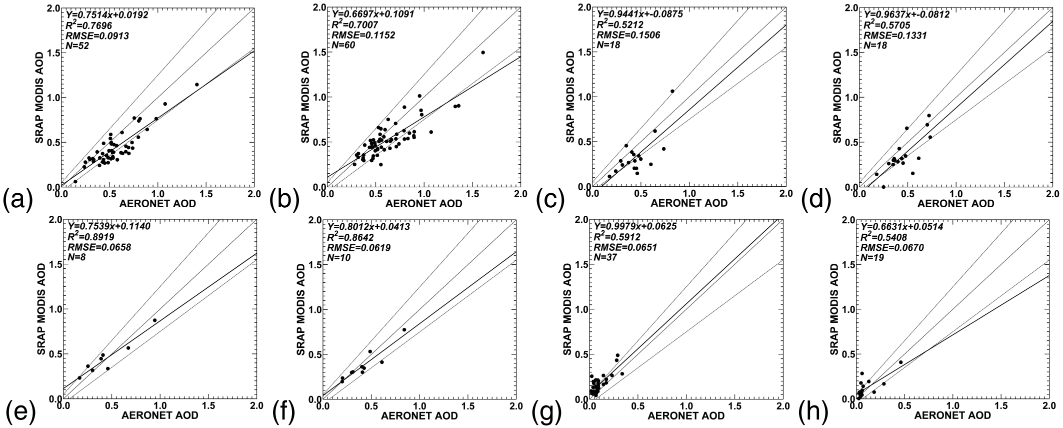

Fig. 5. Relationships between monthly averaged SRAP AODs and monthly averaged AERONET AODs at 550 nm, with a resolution of 10 km × 10 km in different AERONET sites from 2002 to 2011: **(a)** Terra – XiangHe **(b)** Aqua – XiangHe **(c)** Terra – Hong_Kong_ Hok_Tsui **(d)** Aqua – Hong_Kong_ Hok_Tsui **(e)** Terra – Beijing **(f)** Aqua – Beijing **(g)** Terra – Lulin **(h)** Aqua – Lulin.

AMTD

4, 6643–6678, 2011

Long-term aerosol optical depth datasets over China

Y. Xue et al.

Title Page
Abstract | Introduction
Conclusions | References
Tables | Figures
◂◂ | ▸▸
◂ | ▸
Back | Close
Full Screen / Esc
Printer-friendly Version
Interactive Discussion

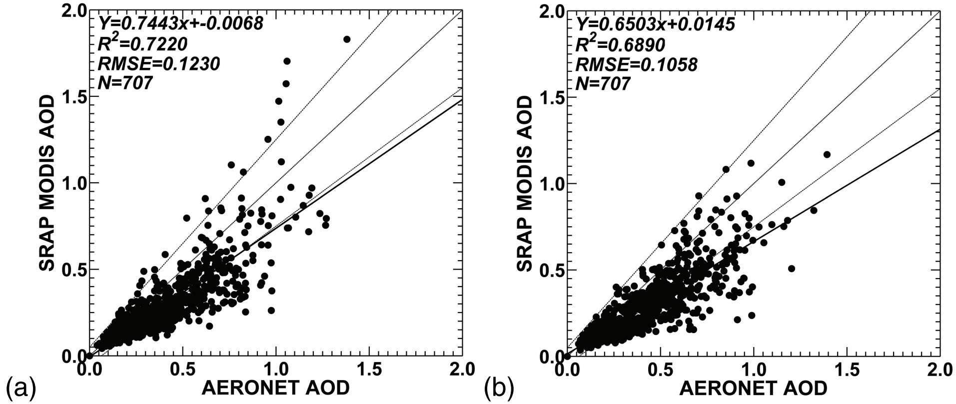

Fig. 6. Relationships between monthly averaged SRAP AODs and monthly averaged AERONET AODs at 550 nm, with a resolution of 10 km × 10 km in Asia for 2002 to 2011: **(a)** Terra and **(b)** Aqua.

AMTD
4, 6643–6678, 2011

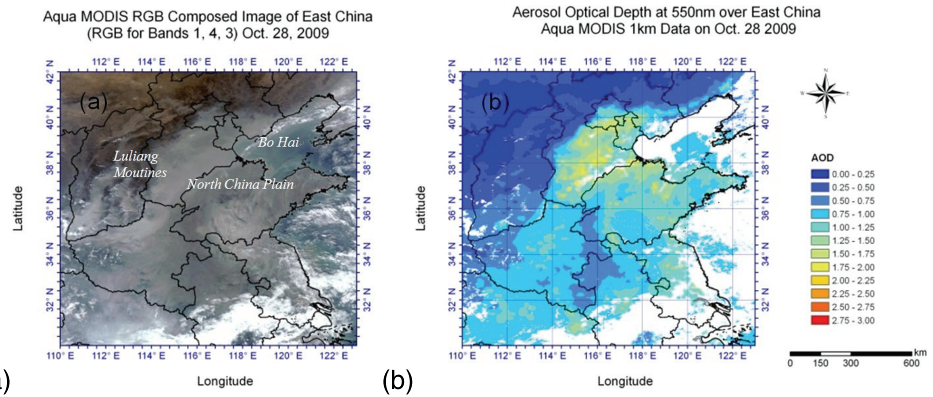

(a) (b)

Fig. 7. (a) Aqua MODIS RGB composed image (R for Band 1; G for Band 4; B for Band 3), Gaussian enhancement is made. **(b)** AODs at 550 nm retrieved by SRAP algorithm from Aqua MODIS data.

AMTD
4, 6643–6678, 2011

Title Page
Abstract Introduction
Conclusions References
Tables Figures
◀◀ ▶▶
◀ ▶
Back Close
Full Screen / Esc
Printer-friendly Version
Interactive Discussion

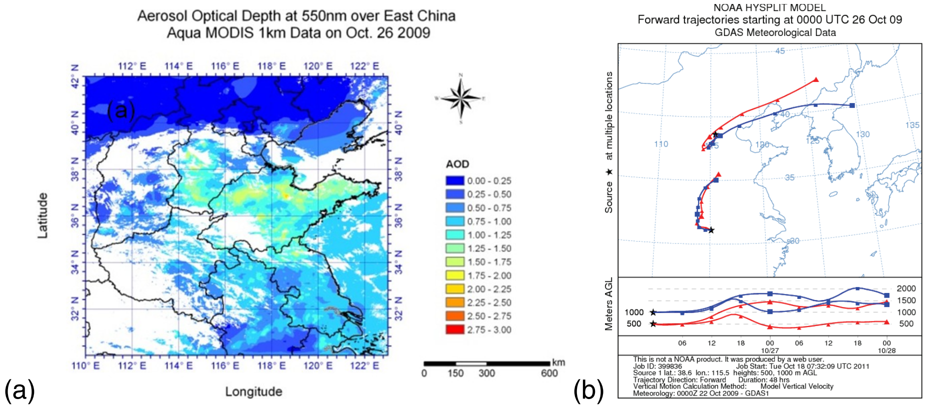

Fig. 8. **(a)** AODs at 550 nm retrieved by SRAP algorithm from Aqua MODIS data on 26 October 2009; **(b)** air mass backward trajectories that originated from Hebei province (38.6° N, 115.5° E), Hubei province (31.1° N, 115.1° E) and Guangdong province (24.9° N, 115.7° E) begin at 00:00 UTC, 26 October 2009. The original points are shown by a star, with 6 h interval.

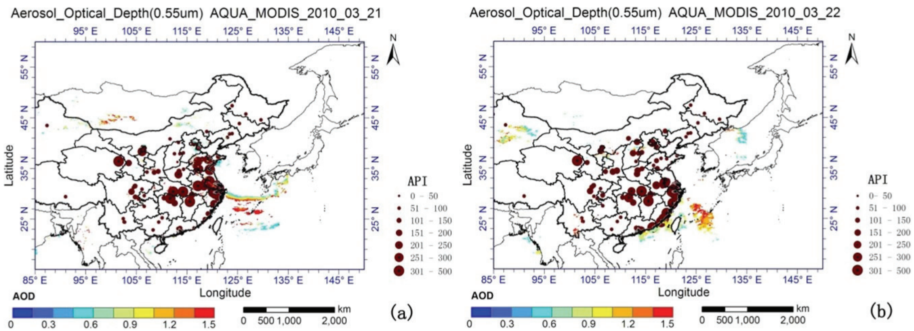

Fig. 9. **(a)** 21 March 2010 **(b)** 22 March 2010 the dust – type AOD distribution and API value of 86 cities superposition chart.

AMTD
4, 6643–6678, 2011

Long-term aerosol optical depth datasets over China

Y. Xue et al.

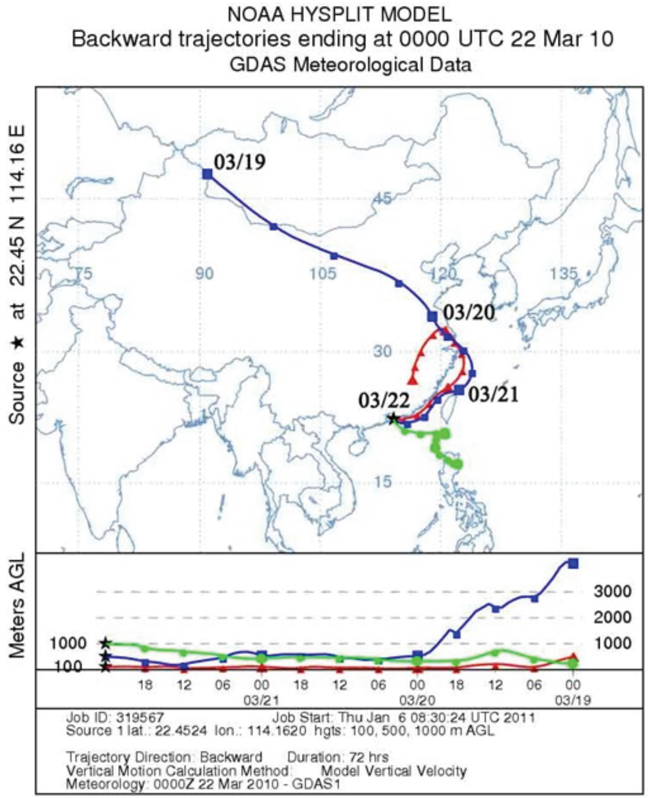

Fig. 10. Air mass backward trajectories of 72-h HYSPLIT-4 on 22 March 2010 at different altitudes with the source region of Hong Kong. Solid circular point, triangle, and square denote a 100 m (red), 500 m (green), and 1000 m (blue) altitude starting point, respectively, with 6-h intervals.

AMTD
4, 6643–6678, 2011

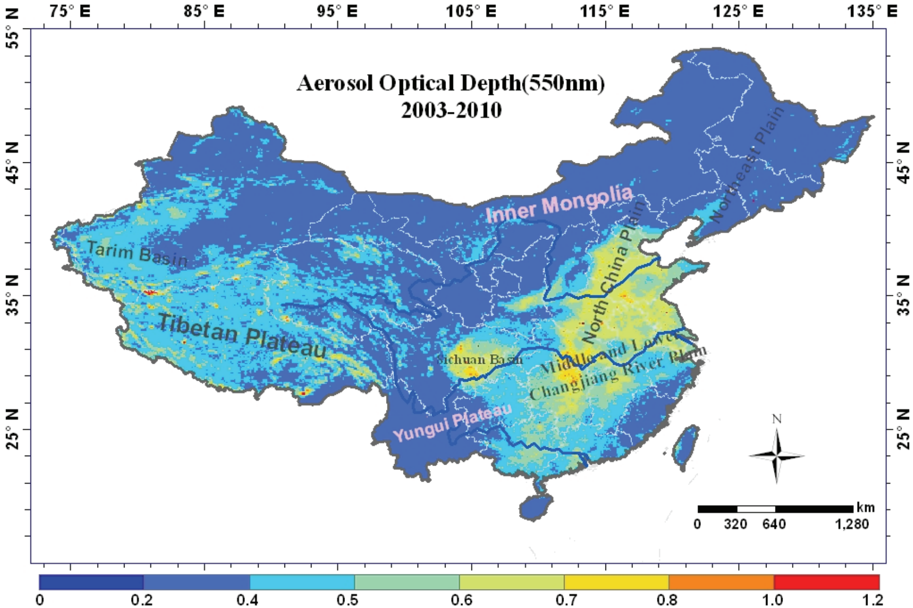

Fig. 11. The distribution of AODs over China averaged from SRAP AOD dataset in the period of 2003–2010.

AMTD
4, 6643–6678, 2011

Title Page
Abstract | Introduction
Conclusions | References
Tables | Figures
◀| |▶
◀ ▶
Back | Close
Full Screen / Esc
Printer-friendly Version
Interactive Discussion

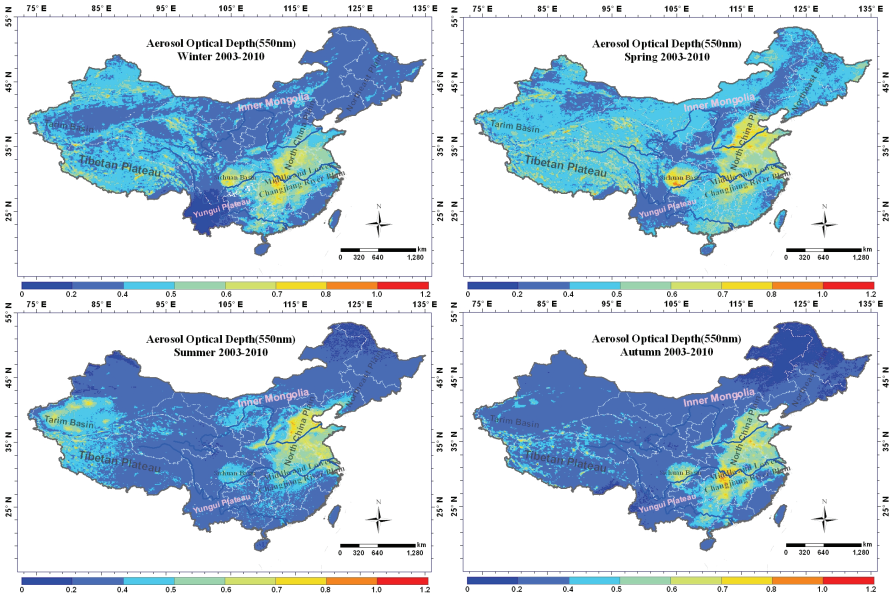

Fig. 12. The four-season distribution of AODs over China averaged from SRAP AOD dataset in the period of 2003–2010.

AMTD
4, 6643–6678, 2011

Long-term aerosol optical depth datasets over China

Y. Xue et al.

Title Page
Abstract Introduction
Conclusions References
Tables Figures
◀◀ ▶▶
◀ ▶
Back Close
Full Screen / Esc
Printer-friendly Version
Interactive Discussion

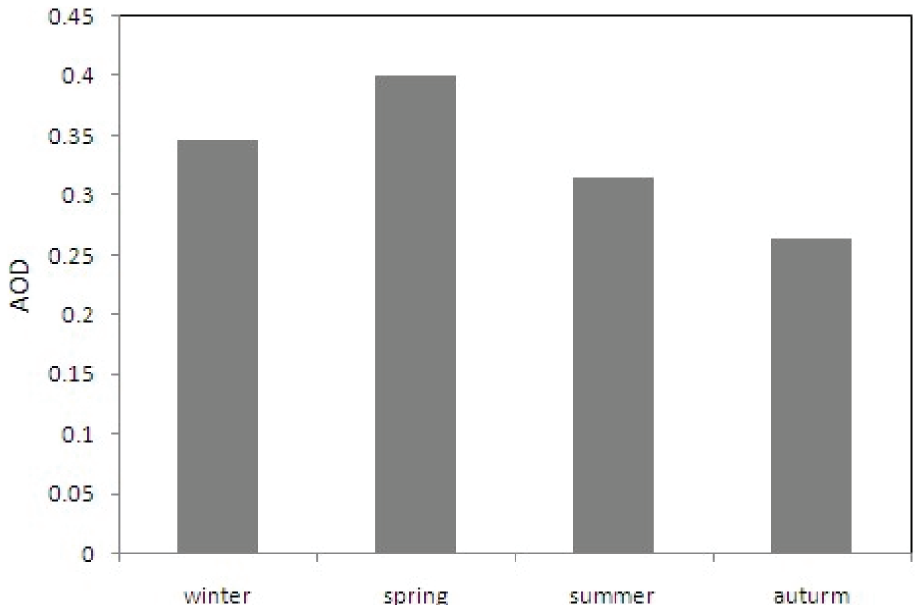

Fig. 13. Column plot of seasonally averaged AODs at 0.55 nm from SRAP AOD dataset in the period of 2003–2010.

AMTD
4, 6643–6678, 2011

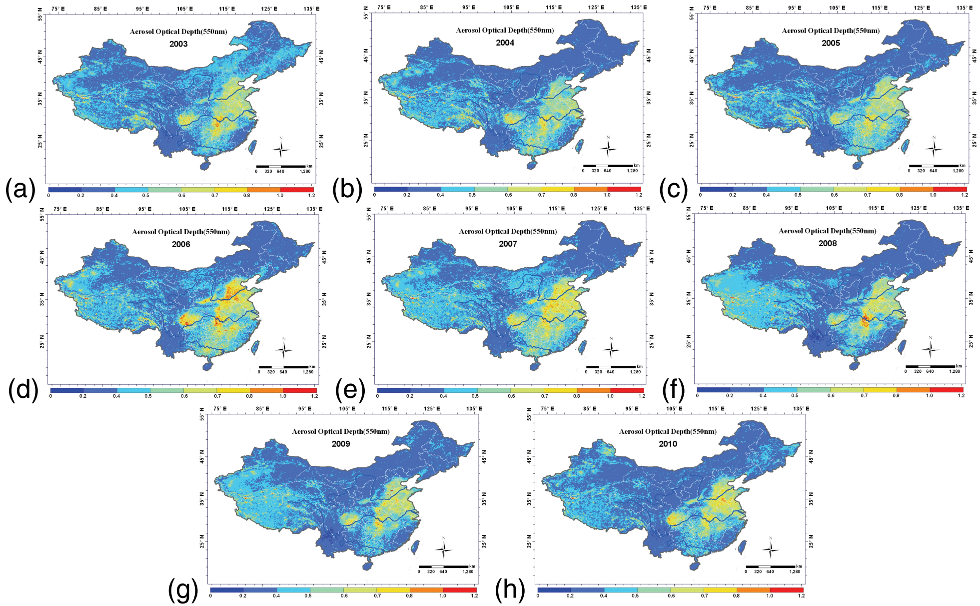

Fig. 14. Annual mean SRAP AOD data for 2003–2010.

AMTD
4, 6643–6678, 2011

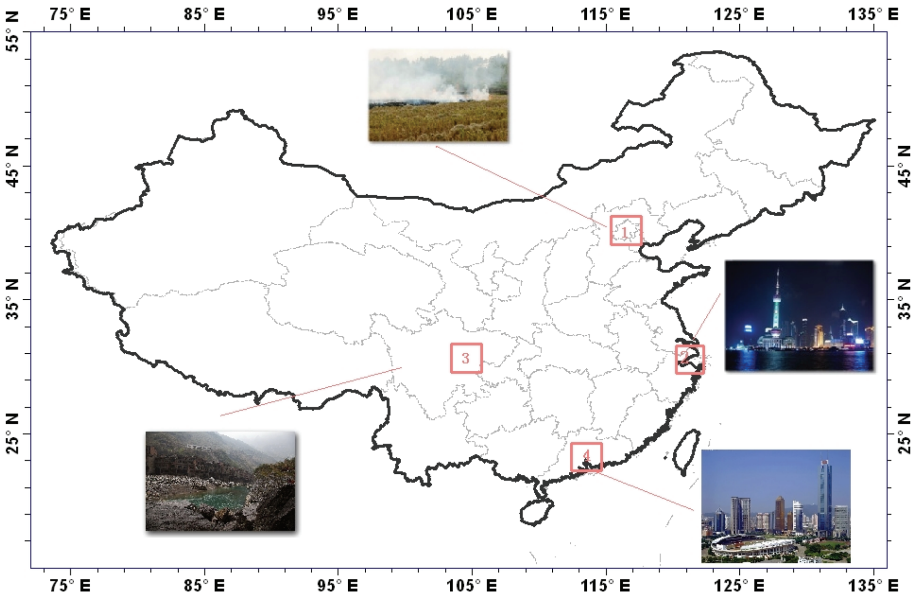

Fig. 15. R1: longitude = [115° E, 117° E], latidude = [39° N, 41° N]; R2: longitude = [120° E, 122° E], latidude = [30° N, 32° N]; R3: longitude = [103° E, 105° E], latidude = [30° N, 32° N]; R4: longitude = [112° E, 114° E], latidude = [22° N, 24° N]. Four regions in China selected for the analysis of the annually variation of AODs.

AMTD
4, 6643–6678, 2011

Long-term aerosol optical depth datasets over China

Y. Xue et al.

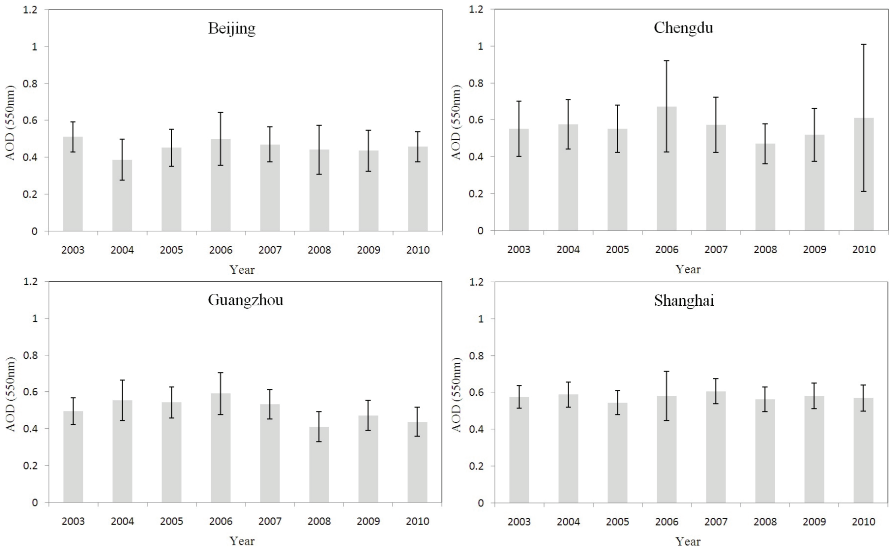

Fig. 16. Column plot of the AODs for 2003–2010 at four regions: Beijing, Shanghai, Chengdu and Guangzhou. The vertical bar line is ± standard deviation.

AMTD
4, 6643–6678, 2011

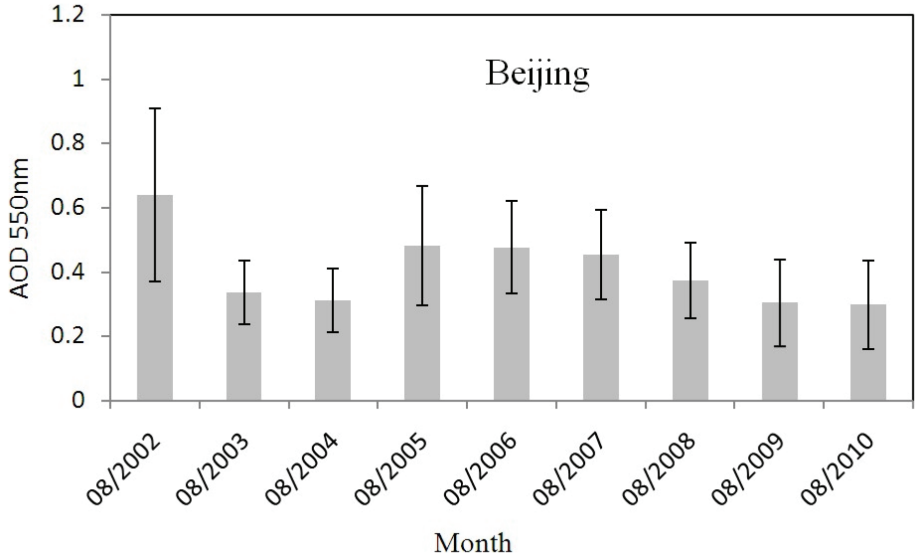

Fig. 17. Column plot of the AODs in Beijing for August 2002 to August 2010. The vertical bar line is ± standard deviation.